General Disclaimer

One or more of the Following Statements may affect this Document

- This document has been reproduced from the best copy furnished by the organizational source. It is being released in the interest of making available as much information as possible.

- This document may contain data, which exceeds the sheet parameters. It was furnished in this condition by the organizational source and is the best copy available.

- This document may contain tone-on-tone or color graphs, charts and/or pictures, which have been reproduced in black and white.

- This document is paginated as submitted by the original source.

- Portions of this document are not fully legible due to the historical nature of some of the material. However, it is the best reproduction available from the original submission.

NASA Technical Memorandum 83366

Vapor Cavitation in Dynamically Loaded Journal Bearings

Bo O. Jacobson
University of Luleå
Luleå, Sweden

and

Bernard J. Hamrock
Lewis Research Center
Cleveland, Ohio

Prepared for the
Second International Conference on Cavitation
sponsored by the Institution of Mechanical Engineers
Edinburgh, Scotland, September 5-8, 1983

NASA

VAPOR CAVITATION IN DYNAMICALLY LOADED JOURNAL BEARINGS

Bo O. Jacobson
University of Luleå
Luleå, Sweden
and
Bernard J. Hamrock
National Aeronautics and Space Administration
Lewis Research Center
Cleveland, Ohio 44135

SYNOPSIS High-speed motion picture camera experiments on dynamically loaded journal bearings revealed the development of vapor cavitation. The parameters studied were the length-to-diameter (L/D) ratio of the bearing, the surface velocities of the journal and bearing, the surface material of the roller, and the static and dynamic eccentricities of the bearing. One hundred and thirty-four cases were filmed. The occurrence of vapor cavitation is clearly evident in the films. Vapor cavitation occurred when the tensile stress applied to the oil exceeded the tensile strength of the oil or the binding of the oil to the surface. The physical situation necessary for vapor cavitation to exist was a squeezing and sliding motion within a bearing.

Besides accurately capturing the cavitation event on film, we analyzed the formation and collapse of the cavitation bubbles. The analysis of the formation of vapor cavitation considered the squeezing and sliding terms of the Reynolds equation while neglecting the Poiseuille terms. A simple criterion for the speeds and eccentricity of the journal and bearing that defines whether vapor cavitation will occur is given by $\varepsilon_d > \omega_s/(2\omega_d)$. The physical implication of the results as they apply to squeeze film dampers is that, if the sliding velocity of the journal is increased, the occurrence of vapor cavitation is decreased. When considering the collapse of the vapor cavitation bubbles, the Poiseuille terms become significant. However, from the experiments the form of the vapor cavitation zone indicates that a short bearing approximation theory could be applied at small L/D.

1 INTRODUCTION

Cavitation is the disruption of a continuous liquid phase by the emergence of gas or vapor. Vapor cavitation is defined as cavitation where the cavitation bubbles contain mainly vapor, and gas cavitation is defined as cavitation where the cavitation bubbles contain mainly noncondensing gas. Understanding the cavitation phenomenon in bearings has been a challenge to tribologists ever since Osborne Reynolds first introduced the subject in his classic 1886 paper. The work in the early 1930's by Swift and Stieber went far in the development of our present understanding of cavitation. Swift (1932) working from stability considerations and Stieber (1933) from flow continuity studies arrived at the same inlet boundary condition:

$$p = p_c \qquad \frac{\partial p}{\partial x} = 0$$

Cavity pressure often differs little from atmospheric pressure and is usually taken as such for the boundary condition. Dowson and Taylor (1975) give an excellent review of the developments in the field of cavitation, beginning with the Swift-Stieber boundary condition and continuing to recent times.

The most common cavitation boundary condition for steadily loaded bearings is the zero-pressure-gradient condition of Swift and Stieber. This condition results from the assumption of continuity of mass flow at the boundary between the cavitation zone and the liquid-filled regions under steady-state conditions. In many bearings, however, dynamic loads cause changes in the local film thickness, and the problem of determining the appropriate boundary condition requires a condition other than zero pressure gradient at the boundary. The studies of Olsson (1965 and 1974) suggest that the usual steady-state condition, $p = dp/dx = 0$, is adequate for dynamic situations if the cavitation boundary moves at a speed that is less than half the journal surface speed. However, if the cavitation boundary moves at a speed that is greater than half the journal surface speed, a more realistic formulation of the boundary condition should be developed. Development of an appropriate cavitation condition for a dynamically loaded journal bearing is one of the objectives of this paper.

In the authors' earlier work (Jacobson and Hamrock, 1982) a high-speed motion picture camera was used to investigate cavitation in dynamically loaded journal bearings. The length-to-diameter ratio of the bearing, the speeds of the journal and bearing, the surface material of the roller, and the static and dynamic eccentricities of the bearing were varied. The results revealed the appearance of previously unsuspected vapor cavitation. Vapor cavitation occurred when the tensile stress applied to the oil exceeded the tensile strength of the oil or the binding of the oil to the surface. The physical situation necessary for vapor cavitation is a squeezing and sliding motion within a bearing. This implies that the minimum film thickness is constantly changing in size and location as a result of the motion tangential and normal to the surfaces.

Having found vapor cavitation in our initial experiments (Jacobson and Hamrock, 1982) we designed, manufactured, and assembled a totally new cavitation rig. The new test rig was developed to more precisely measure the

squeezing and sliding motions with stiffer construction and more accurately manufactured parts. As with the previous work, a high-speed motion picture camera was used to capture the cavitation formation and collapse in dynamically loaded journal bearings. Besides accurately capturing the cavitation event on film, we analyzed the formation and collapse of the cavitation bubbles. That analysis and a description of the characteristics of the bubble content are presented in this paper. From these results a criterion for the occurrence of vapor cavitation is developed for dynamically loaded journal bearings.

2 NOTATION

c	radial clearance, m
D	diameter of bearing, m
d	dynamic eccentricity, m
e	static electricity, m
h	oil film thickness, m
h_{min}	instantaneous minimum oil film thickness, m
L	length of roller, m
p	pressure, N/m^2
p_c	cavitation pressure, N/m^2
p_0	atmospheric pressure, N/m^2
q_c	flow per unit width into vapor cavitation zone, m^2/s
r	radius of roller, m
s	static eccentricity, m
t	time, s
U_a	sliding velocity of journal relative to minimum film thickness, m/s
U_b	sliding velocity of bearing relative to minimum film thickness, m/s
v_c	cavitation boundary velocity, m/s
w	squeeze velocity, m/s
x	coordinate in direction of sliding, m
y	coordinate in surface plane perpendicular to x-axis, m
γ	angle giving location of minimum film thickness, rad
$\dot{\gamma}$	rotational speed of minimum film thickness, rad/s
y_c	cavitation boundary coordinate, m
y_m	roller edge coordinate, m
ϵ_s	static eccentricity ratio
ϵ_d	dynamic eccentricity ratio
η	viscosity, $N\ s/m^2$
μ	instantaneous eccentricity, m
λ	defined by equation (2), m/s
ϕ	coordinate angle from minimum-film-thickness location, rad
ω_d	rotational speed of eccentricity mechanism, rad/s
ω_s	rotational speed of roller, rad/s

3 APPARATUS AND TEST PROCEDURE

The experimental setup with the high-speed camera, motors, and test rig is shown in figure 1. The high-speed motion picture camera that was used could take up to 11 000 frames per second with ordinary 16-mm motion picture film. In the experiments presented in this report the framing rates were 1000 and 2000 frames per second.

The test bearing was lubricated by gravity feed from a can placed approximately 600 mm above the bearing. The test lubricant was a nondegassed Dextron-II type of automatic transmission fluid with a viscosity of 0.066 N s/m^2 at atmospheric conditions. The lubricant passed from the can through a line and entered the bearing at the top left of the polymethylmethacrylate (PMMA) bearing shown in figure 1. At the right of figure 1 is the motor that gives the sliding velocity to the roller, and at the left is the motor that gives the squeeze velocity to the bearing. The speeds of these identical 0.5-kW motors can vary continuously from 0 to 250 rad/s.

Figure 2 shows the PMMA bearing, which can vibrate in a circular motion keeping the axis of vibration parallel to the axis of rotation. The special mechanism manufactured to keep the centerline of the bearing parallel to the centerline of the journal when the bearing is vibrating is shown in figure 2. It consists of three plates each coupled together with four thin plates made from spring steel. The spring steel plates could easily be bent in the direction perpendicular to the plates but were very stiff in the horizontal planes of the plates. Because of the symmetry of the mechanism the thick plates were always parallel to each other when the thin plates were bent as long as they did not buckle.

The dynamic eccentricity mechanism shown assembled in figure 2 is shown isolated in figure 3. The amplitude of the vibration of the squeeze motion is given by the dynamic eccentricity ratio determined from the setting of the parts shown in figure 3. By rotating one part relative to the other the dynamic eccentricity can be varied between 0 and 0.5 mm. Since the radial clearance is 0.5 mm, the ratio ϵ_d of the dynamic eccentricity to the radial clearance can be varied between 0 and 1. By setting the dynamic eccentricity equal to zero and moving the journal relative to the centerline of the bearing, the static eccentricity can be varied between 0 and 0.5 mm, meaning that the static eccentricity ratio ϵ_s can be varied between 0 and 1. Therefore the offset of the center of vibration from the center of the journal gives a static load, and the amplitude of the vibration gives a variable rotating dynamic load superimposed on the static load. Both the location of the center of vibration and the amplitude of vibration can vary.

Figure 4 shows four positions of the journal relative to the bearing for a dynamically loaded journal bearing. The static eccentricity ratio ϵ_s is set at 0.4, and the dynamic eccentricity ratio ϵ_d is set at 0.6. The direction of the dynamic eccentricity rotates 90° counterclockwise going from (a) to (b), (b) to (c), and (c) to (d). In figure 4 the squeeze component of motion is clearly visible.

The following ranges of conditions were considered:

(1) Bearing L/D ratios of 1, 1/2, and 1/4
(2) Eccentricity ratios:
    (a) $\epsilon_d = 0.414$ and $\epsilon_s = 0.586$
    (b) $\epsilon_d = 0.660$ and $\epsilon_s = 0.340$
(3) Roller surface materials of steel and polytetrafluoroethylene (PTFE)
(4) Six motor speeds, ranging from 19.5 to 104 rad/s

One hundred and thirty-four cases were filmed.

4 EXPERIMENTAL RESULTS

Figure 5 presents several frames from the high-speed films showing the formation and collapse of vapor cavitation in a journal bearing. The actual film provides a better illustration; however, the figures highlight the film. The fixed conditions for figure 5 are L/D = 1/4, ϵ_s = 0.340, ϵ_d = 0.660, ω_s = 19.5 rad/s, ω_d = 92.7 rad/s, and PTFE journal surface. The framing rate of the camera was 2000 frames/s. The time from the first frame to the last in figure 5 was less than 20 ms, indicating how rapidly the vapor cavitation forms and collapses.

The sample frames of the 134 cases filmed (fig. 5) illustrate that in dynamically loaded journal bearings cavitation bubbles containing mainly oil vapor are present. To the authors' knowledge, other than our initial report (Jacobson and Hamrock, 1982), this was never shown before. Vapor cavitation is quite different from gas cavitation. The gas cavitation bubbles can be transported through the high-pressure region of the bearing as demonstrated in Jacobson and Hamrock (1982). On the other hand, vapor cavitation bubbles dissolve and disappear in less than a hundredth of a cycle of vibration (less than a millisecond). Without a high-speed camera one would not be able to observe vapor cavitation. Furthermore, this type of cavitation can cause erosive wear of adjacent surfaces, so its presence in dynamically loaded journal bearings is an important observation.

A photograph was taken of the frame that produced the maximum vapor cavitation for each of the 134 cases filmed. Some of the interesting observations from these photographs are shown in figures 6 to 9 and are discussed below. Remember that each of these figures was obtained from the frame of the film that produced the largest vapor cavitation zone for the particular case being studied.

4.1 Effect of roller material

Figure 6(a) presents dynamic cavitation bubble development for a PTFE roller, and 6(b) for a steel roller, when all the other parameters were kept constant. The vapor cavitation zone was wider for the PTFE journal than for the steel roller. This can be the result of the steel roller's higher surface energy. The inner structures of the vapor cavitation zone were quite different for the two rollers, especially in the downstream part. This is no doubt due to the rollers different surface energies; that is, PTFE was not wetted by the oil, but the steel was.

The film indicates that two mechanisms start vapor cavitation. One of the mechanisms occurs when the binding between the oil and the journal surface is weaker than the oil. Here vapor cavitation starts in the same position for each cycle of the squeeze motion. The other occurs when the oil is weaker than the binding between the oil and the journal surface. In this case, the small impurities within the oil (such as dirt or gas bubbles) determine where cavitation starts.

4.2 Influence of length-to-diameter ratio

Figure 7 shows the effect on the vapor cavitation zone of L/D of 1, 1/2, and 1/4 when the other parameters were kept constant. The total area of the vapor cavitation zone seems to be independent of L/D. However, the width of the cavitation zone relative to the width of the journal decreased as L/D increased, going from 75 percent for L/D = 1/4 to 50 percent for L/D = 1. For L/D = 1 elastic distortion of the bearing could alter the geometry of the bearing as the force is proportional to $(L/D)^2$.

4.3 Effect of eccentricity ratios

Figure 8 shows the influence of two combinations of dynamic and static eccentricity ratios (ϵ_d and ϵ_s) on vapor cavitation. In figure 8(a) ϵ_d = 0.414 and ϵ_s = 0.586, and in figure 8(b) ϵ_d = 0.660 and ϵ_s = 0.340 while the other parameters were kept constant. The vapor cavitation zone increased roughly proportional to ϵ_d.

4.4 Influence of speed

Figure 9 shows the influence of two rotational speeds of the eccentric, giving two different squeeze velocities, on the size of the vapor cavitation zone. In figure 9(a) ω_d = 27.8 rad/s, and in figure 9(b) ω_d = 92.7 rad/s. For the higher squeeze velocity the bubble size increased significantly. Below a certain squeeze velocity no vapor cavitation was found. Furthermore, it was generally concluded that if the sliding velocity was increased, the squeeze velocity had to be increased proportionately in order to maintain the same amount of vapor cavitation. The results are explained in the theory, equations (2) to (16). The physical implication of the results as they apply to squeeze film dampers is that, if the sliding velocity is increased, the occurrence of vapor cavitation is decreased.

5 THEORY

The appropriate Reynolds equation when considering sliding and squeezing motion as experienced in the test apparatus can be written as

$$\frac{\partial}{\partial x}\left(h^3 \frac{\partial p}{\partial x}\right) + \frac{\partial}{\partial y}\left(h^3 \frac{\partial p}{\partial y}\right) - 6\eta(U_a + U_b)\frac{\partial h}{\partial x} - 12\eta \frac{\partial h}{\partial t} = 0 \qquad (1)$$

where

U_a sliding velocity of journal relative to minimum film thickness, m/s

U_b surface velocity of bearing relative to minimum film thickness, m/s

In equation (1) it is assumed that the fluid is incompressible and isoviscous. The first two terms in equation (1) are the Poiseuille terms and describe the net flow rates due to the pressure gradients within the lubricated area. The second of these terms is referred to as the side leakage term since it describes the net flow due to the pressure gradient along the axis of the bearing, transverse to the direction of sliding. The third term describes the net entraining flow rate due to the sliding velocities of the surfaces and is referred to as the sliding term. The fourth term describes the net flow rate due to the

squeeze motion and is referred to as the squeeze term.

5.1 Cavitation formation

The two most significant terms of the Reynolds equation when considering the formation of vapor cavitation are the sliding and squeeze terms. Therefore we can define a parameter λ that essentially describes the sliding and squeezing motion as

$$\lambda = \frac{(U_a + U_b)}{2}\frac{\partial h}{\partial x} + \frac{\partial h}{\partial t} \tag{2}$$

The angle γ shown in figure 4(b) is shown in more detail in figure 12. From this figure γ can be written as

$$\gamma = \tan^{-1}\left[\frac{\epsilon_d \sin(\omega_d t)}{\epsilon_s + \epsilon_d \cos(\omega_d t)}\right] \tag{3}$$

where $\epsilon_d = d/c$ and $\epsilon_s = s/c$. The angular velocity of the minimum film thickness can be written as

$$\dot{\gamma} = \frac{\epsilon_d[\epsilon_s \cos(\omega_d t) + \epsilon_d]\,\omega_d}{\epsilon_s^2 + \epsilon_d^2 + 2\epsilon_s\epsilon_d \cos(\omega_d t)} \tag{4}$$

Figure 11(a) shows the geometry of the journal and the bearing as it appears in the test rig. The minimum film thickness rotates around the bearing and its location is denoted by γ. Figure 11(b) shows the geometry when the rotational speed $-\dot{\gamma}$ is superimposed on the sliding velocities of the journal and the bearing. The minimum film thickness remains in the same location in this coordinate system. From this figure the sliding velocities of the journal and bearing can be written as

$$U_a = \omega_s r - \dot{\gamma} r \tag{5}$$

$$U_b = -\dot{\gamma}(r + h)\cos\left(\frac{u \sin\varphi}{r}\right) - \omega_d d \sin(\omega_d t - \gamma)\sin\varphi \tag{6}$$

where r is the radius of the roller. The value of $\cos(u \sin\varphi/r)$ is very close to unity, and h is much less than r. In writing equation (6) it is also assumed that $d\omega_d$ is much smaller than $r\omega_s$ since typically $d\omega_d$ is at least one order of magnitude smaller than $r\omega_s$. Therefore equation (6) reduces to

$$U_b = -\dot{\gamma} r \tag{7}$$

From figure 4(b) the equation for the instantaneous film thickness can be written as

$$h = c - \mu \cos\varphi \tag{8}$$

where

$$\mu = \frac{d \sin(\omega_d t)}{\sin\gamma} \tag{9}$$

In figures 4(b) and 10, μ is the instantaneous distance between the center of the journal and the center of the bearing. The instantaneous minimum film thickness occurs where the coordinate angle $\varphi = 0$ or

$$h_{min} = c - \mu \tag{10}$$

Knowing the film thickness, we can write the squeeze velocity as

$$W = \frac{d\epsilon_s\epsilon_d\omega_d \sin^2(\omega_d t)\cos\varphi}{\sin\gamma\,[\epsilon_s^2 + \epsilon_d^2 + 2\epsilon_s\epsilon_d\cos(\omega_d t)]} \tag{11}$$

also

$$\frac{\partial h}{\partial x} = \frac{1}{r}\frac{\partial h}{\partial \varphi} = \mu \sin\frac{\varphi}{r} \tag{12}$$

Substituting equations (5), (6), (11), and (12) into equation (2) gives

$$\lambda = \frac{\mu}{2}(\omega_s - 2\dot{\gamma})\sin\varphi + \frac{d\epsilon_s\epsilon_d\omega_d \sin^2(\omega_d t)\cos\varphi}{\sin\gamma\,[\epsilon_s^2 + \epsilon_d^2 + 2\epsilon_s\epsilon_d\cos(\omega_d t)]} \tag{13}$$

In the experiments it was observed that vapor cavitation only occurred when μ approached the radial clearance c. This implies that the time t in equation (13) is close to zero and $\cos(\omega_d t) = 1$ and $\sin(\omega_d t) = \omega_d t$. With these substitutions equation (13) reduces to

$$\lambda = c\left\{\sin\varphi\left[\frac{\omega_s(\epsilon_s + \epsilon_d)}{2} - \epsilon_d\omega_d\right] + \frac{\epsilon_s\epsilon_d\omega_d^2 t\cos\varphi}{\epsilon_s + \epsilon_d}\right\} \tag{14}$$

Note that the first expression in equation (14) is not a function of t. Therefore for small values of t equation (14) reduces to

$$\lambda = c \sin\varphi\left[\frac{\omega_s(\epsilon_s + \epsilon_d)}{2} - \epsilon_d\omega_d\right] \tag{15}$$

If, when t approaches zero, the minimum film thickness is small enough ($h_{min} < 0.1\,c$), there will always be vapor cavitation if $\lambda > 0$. Since the films indicate that vapor cavitation occurred for negative φ relative to the minimum film thickness, where motor speed is in the positive φ direction, the criterion for the formation of vapor cavitation is

$$\epsilon_c > \frac{\omega_s}{2\omega_d} \tag{16}$$

where $\epsilon_s + \epsilon_d = 1$.

5.2 Cavitation collapse

Once vapor cavitation has formed and some time has passed, the minimum film thickness increases and the atmospheric pressure at the edges of the bearing becomes important for con-

sideration of the collapse of the vapor cavitation bubbles. Recalled from equation (1) that for increasing film thickness the Poiseuille terms, which contain the pressure gradient multiplied by the film thickness cubed, must be considered. The high-speed films showed that the shape of the vapor cavitation zone was longer in the rolling direction than in the transverse, especially for narrow bearings. Because of this a short bearing type of approach could be used, and the appropriate Reynolds equation for considering the vapor cavitation collapse is

$$\frac{\partial}{\partial y}\left(h^3 \frac{\partial p}{\partial y}\right) = 6\eta(U_a + U_b)\frac{\partial h}{\partial x} + 12\eta \frac{\partial h}{\partial t} \qquad (17)$$

Figure 12 shows the geometry of the collapsing vapor cavitation zone. The pressure within the vapor cavitation zone is p_c and that at the ends of the journal is atmospheric, p_0. Therefore integrating equation (17) twice while making use of figure 12 in defining the boundary conditions gives

$$p - p_0 = \frac{(y - y_c)(y - y_m)}{2} \times\left[\frac{6\eta}{h^3}(U_a + U_b)\frac{\partial h}{\partial x} + \frac{12\eta}{h^3}\frac{\partial h}{\partial t}\right] + \frac{p_c - p_0}{y_c - y_m}(y - y_m) \qquad (18)$$

The flow rate into the vapor cavitation zone at $y = y_c$ can be written as

$$q_c = \left(\frac{h^3}{12\eta}\frac{\partial p}{\partial y}\right)_{y=y_c} \qquad (19)$$

The average velocity at this boundary if the film thickness in the bubble approaches zero is

$$v_c = \frac{q_c}{h} = \frac{h^2}{12\eta}\left(\frac{\partial p}{\partial y}\right)_{y=y_c} \qquad (20)$$

Making use of equation (18) while obtaining the pressure gradient at the cavitation boundary and substituting it in equation (20) gives

$$v_c = \frac{(y_c - y_m)}{2h} \times\left[\frac{(U_a + U_b)}{2}\frac{\partial h}{\partial x} + \frac{\partial h}{\partial t}\right] + \frac{h^2}{12\eta}\frac{(p_0 - p_c)}{(y_m - y_c)} \qquad (21)$$

The vapor cavitation zone is collapsing when $v_c > 0$:

$$-\frac{(y_m - y_c)}{2h} \times\left[\frac{(U_a + U_b)}{2}\frac{\partial h}{\partial x} + \frac{\partial h}{\partial t}\right] + \frac{h^2}{12\eta}\frac{(p_0 - p_c)}{(y_m - y_c)} > 0 \qquad (22)$$

or the maximum sum of the sliding and squeeze velocities for the collapse of the vapor cavitation is

$$\frac{(U_a + U_b)}{2}\frac{\partial h}{\partial x} + \frac{\partial h}{\partial t} < \frac{h^3}{6\eta}\frac{(p_0 - p_c)}{(y_m - y_c)^2} \qquad (23)$$

6 SUMMARY OF RESULTS

The occurrence of vapor cavitation is clearly evident in the films as well as in the figures, which were directly obtained from the films. Vapor cavitation occurred when the tensile stress applied to the oil exceeded the tensile strength of the oil or the binding of the oil to the surface. The physical situation necessary for vapor cavitation to exist was a squeezing and sliding motion within a bearing. A simple criterion for the speeds and eccentricity of the journal and bearing that defines whether vapor cavitation will occur is given by $\epsilon_d > \omega_s/(2\omega_d)$. The physical implication of the results as they apply to squeeze film dampers is that, if the sliding velocity is increased, the occurrence of vapor cavitation is decreased. When considering the collapse of the vapor cavitation bubbles, the Poiseuille terms become significant. However, from the experiments the form of the vapor cavitation zone indicates that a short bearing approximation theory could be applied for small length-to-diameter ratios.

7 REFERENCES

Dowson, D. and Taylor, C. M.: Fundamental Aspects of Cavitation in Bearings, Cavitation and Related Phenomena in Lubrication, Proceedings of the First Leeds-Lyon Symposium on Tribology, Mechanical Engineering Publication, London, 1975, pp. 15-26.

Jacobson, B. O. and Hamrock, B. J.: High-Speed Motion Picture Camera Experiments of Cavitation in Dynamically Loaded Journal Bearings, presented at the Joint Lubrication Conference, Washington, DC, October 1982, then published in the transaction of ASME, Journal of Lubrication Technology.

Olsson, K. O.: Cavitation of Dynamically Loaded Bearings, Chalmers Tekniska Hogskolas Handlingar, No. 308, 1965, pp. 1-60.

Olsson, K. O.: Theoretical and Experimental Investigation of Pressure Buildup and Cavitation Regions in a Bearing with Stationary Whirl, Ph.D. Thesis, Chalmers Tekniska Hogskola, Gothenburg, Sweden, 1974.

Reynolds, O.: On the Theory of Lubrication and Its Application to Mr. Beauchamp Tower's Experiments, Including an Experimental Determination of Viscosity of Olive Oil, Philosophical Transactions of the Royal Society, London, Vol. A1777, pp. 157-234, 1886.

Stieber, W.: Das Schwimmlager, Hydrodynamische Theorie des Gleitlagers, VDI - Verlag, Berlin, 1933.

Swift, H. W.: The Stability of Lubricating Films in Journal Bearings, Proceedings Institution of Civil Engineers, Vol. 23, No. 4809, pp. 267-288, Discussion pp. 289-322, 1932.

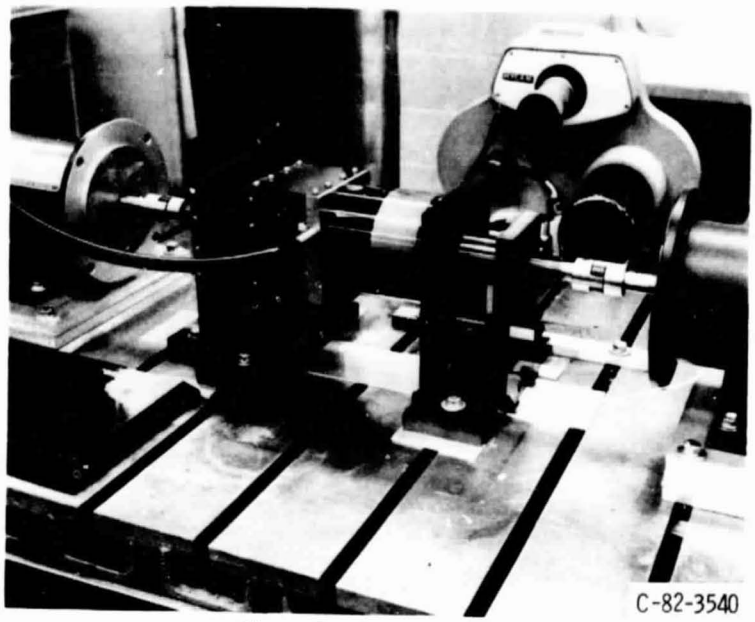

Figure 1. - Test apparatus.

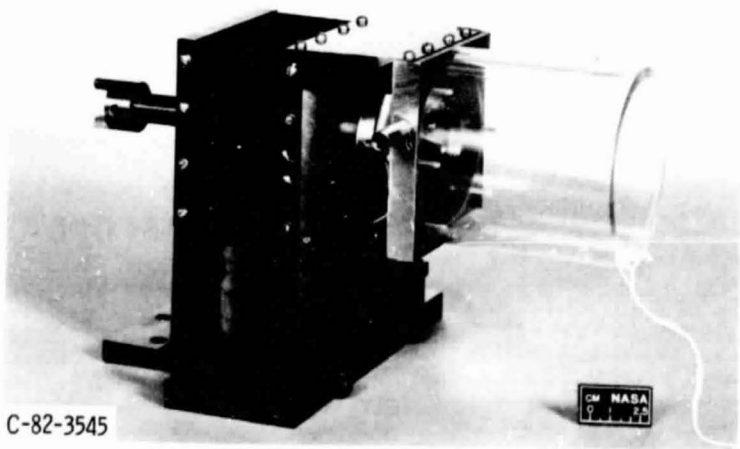

Figure 2. - PMMA-tube and eccentric.

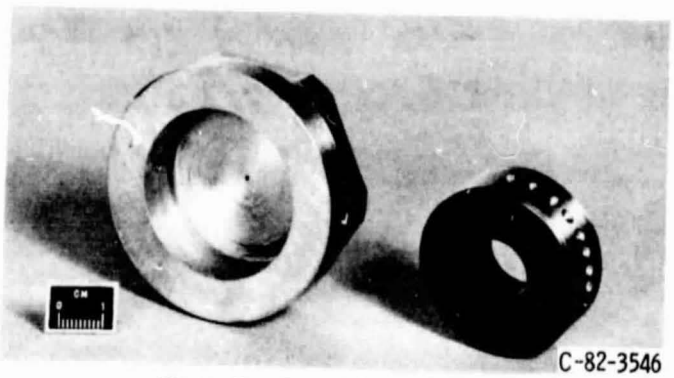

Figure 3. - Eccentric mechanism.

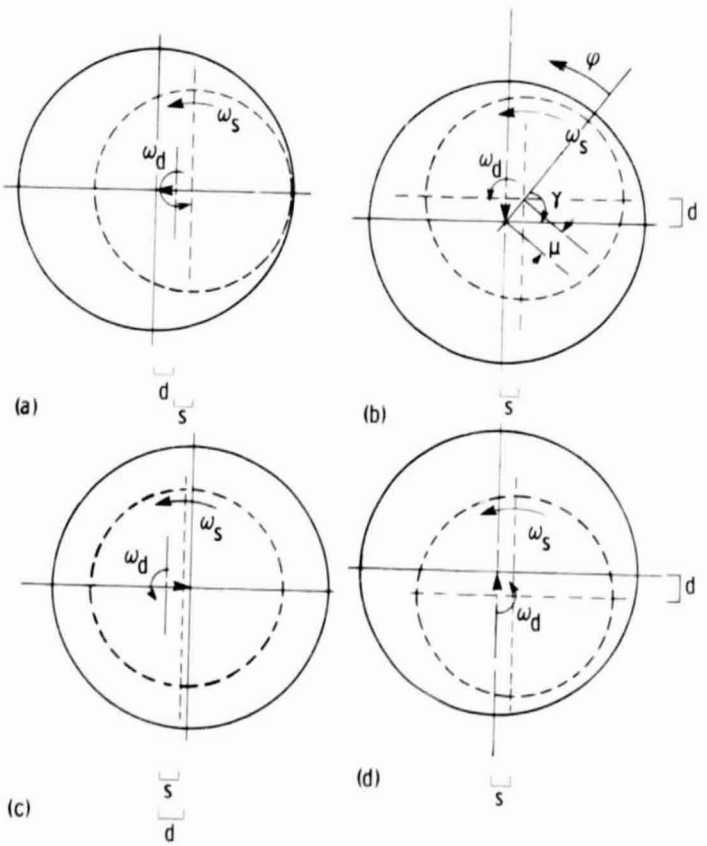

Figure 4. - Bearing geometries at four different times.
$\varepsilon_s = 0.4$; $\varepsilon_d = 0.6$.

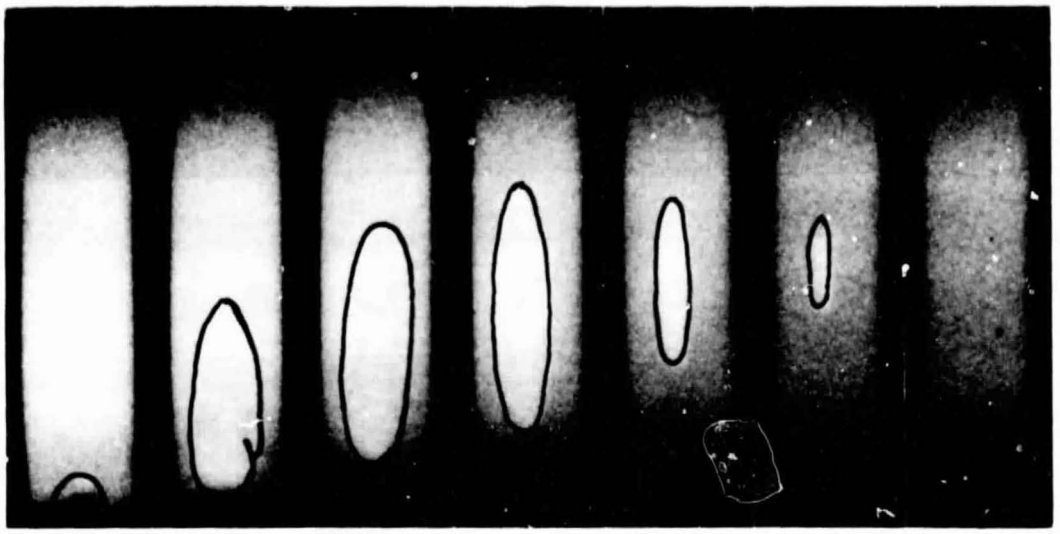

Figure 5. - Dynamic cavitation bubble development. ($\epsilon_s = 0.34$, $\epsilon_d = 0.66$, $\omega_s = 19.5$ rad/s, and $\omega_d = 92.7$ rad/s).

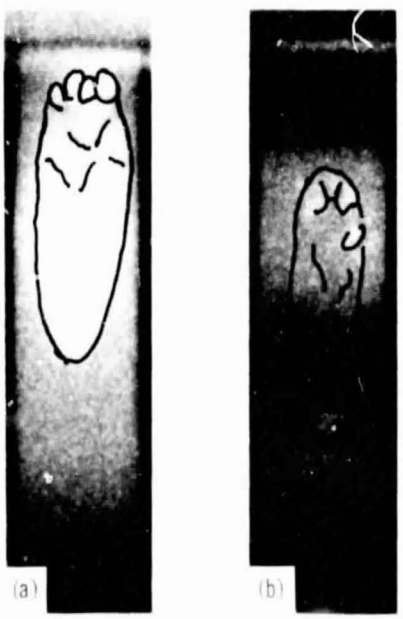

(a) PTFE.

(b) Steel.

Figure 6. - Influence of roller material.

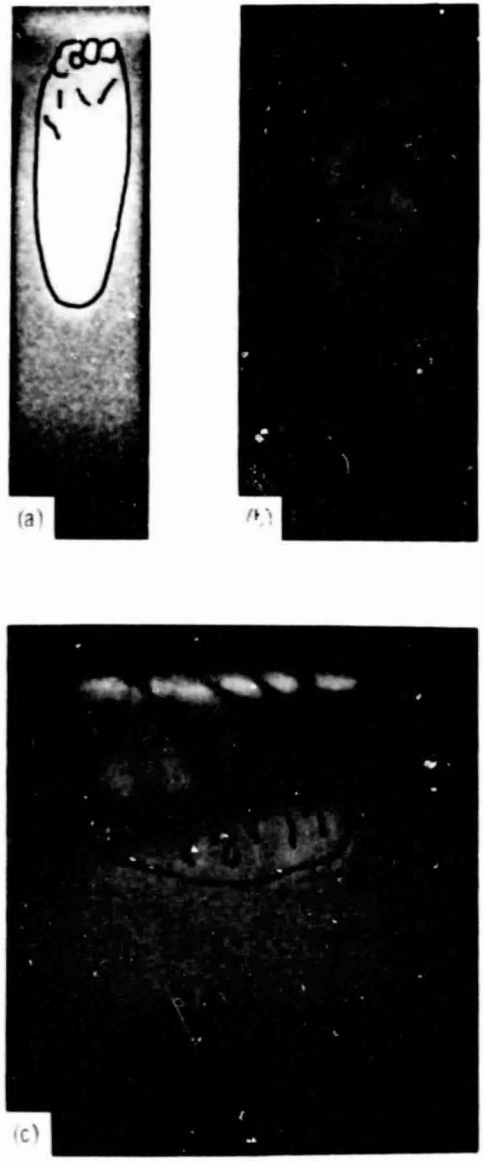

Figure 7. - Influence of length to diameter ratio.

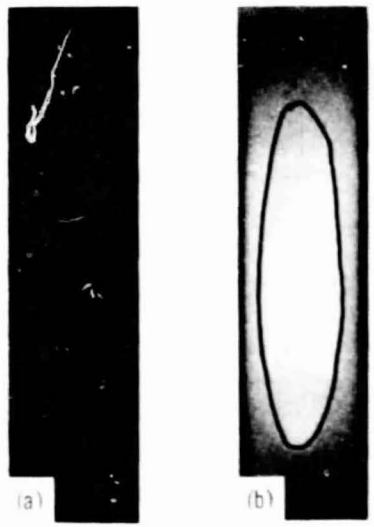

(a) $\epsilon_s = 0.586$, $\epsilon_d = 0.414$

(b) $\epsilon_s = 0.340$, $\epsilon_d = 0.660$

Figure 8. - Influence of eccentricity ratios.

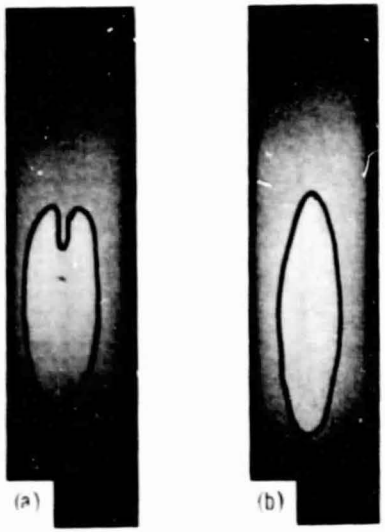

(a) $\omega_S = 19.5$ rad/s, $\omega_d = 27.8$ rad/s

(b) $\omega_S = 19.5$ rad/s, $\omega_d = 92.7$ rad/s

Figure 9. - Influence of speed.

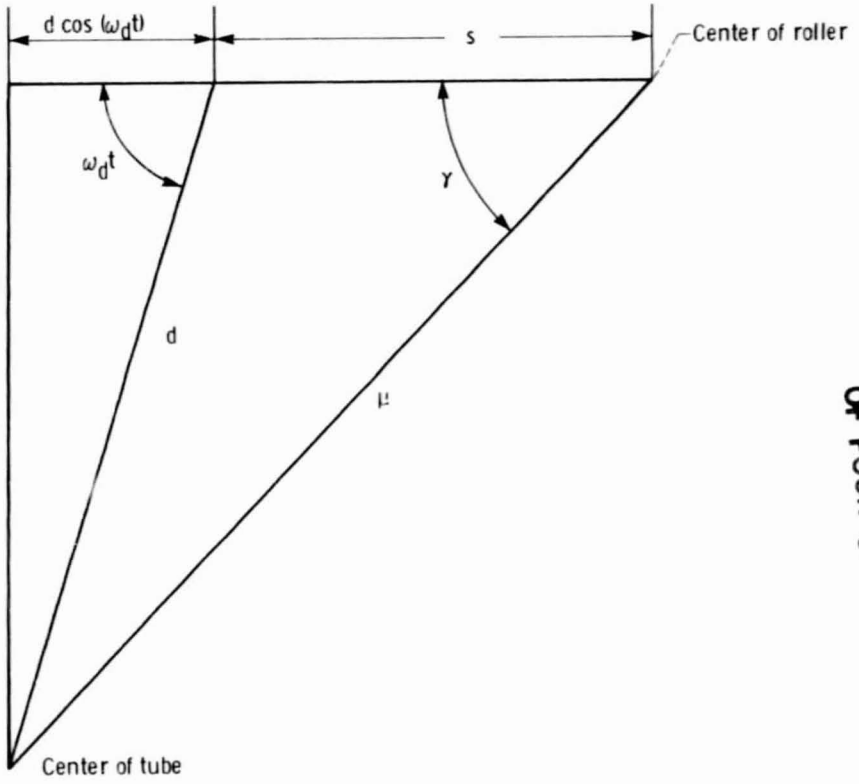

Figure 10. - Geometry of the eccentrics.

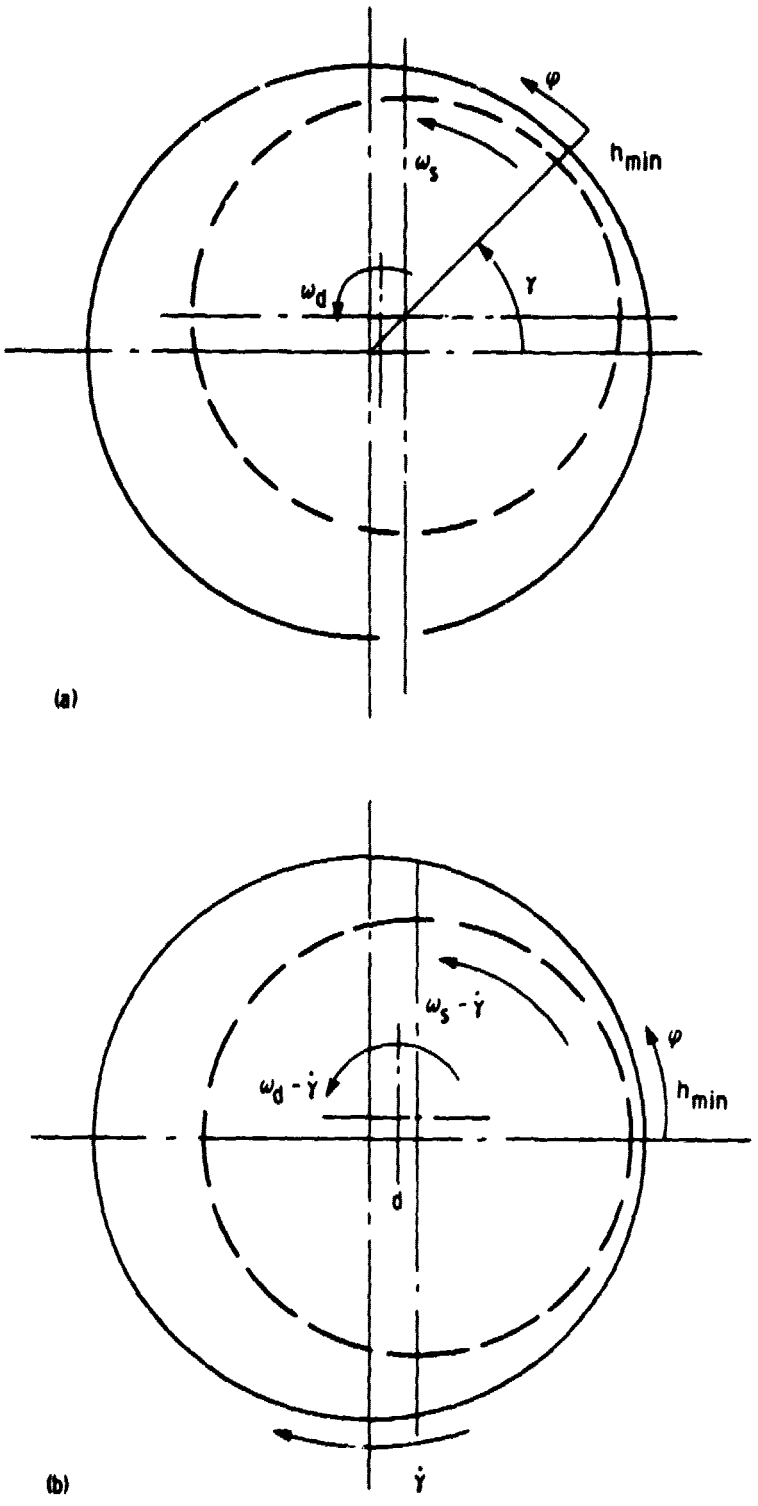

(a) Geometry of roller and tube.

(b) Geometry of roller and tube when rotational speed - $\dot{\gamma}$ is superimposed on sliding velocities of roller and tube.

Figure 11. - Geometry for Reynolds equation.

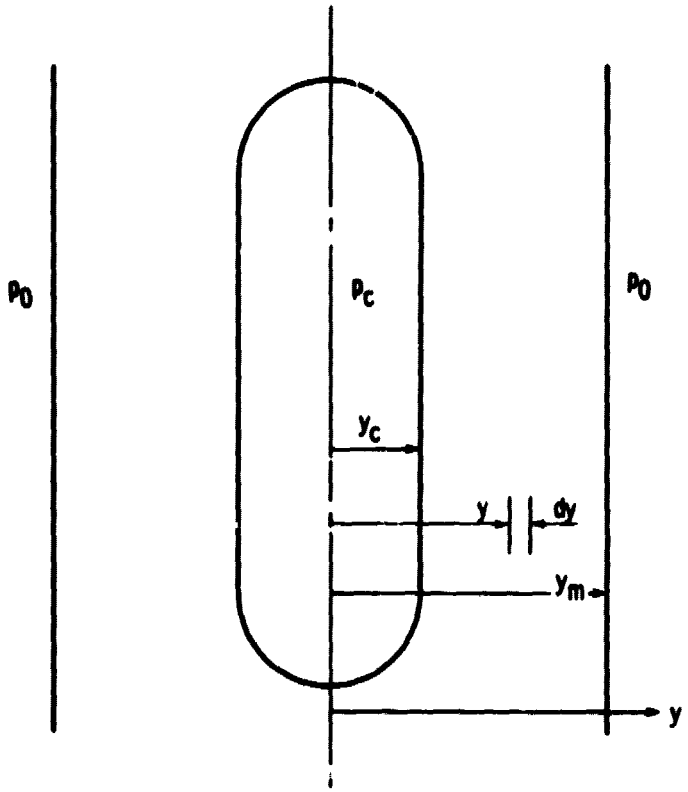

Figure 12 - Geometry of collapsing vapor cavitation zone.